HEALTH AND MEDICINE

CMPK2 and BCL-G are associated with type 1 interferon–induced HIV restriction in humans

Ramy El-Diwany[1,2], Mary Soliman[1], Sho Sugawara[1], Florian Breitwieser[3], Alyza Skaist[4], Candelaria Coggiano[1], Neel Sangal[1], Michael Chattergoon[1], Justin R. Bailey[1], Robert F. Siliciano[1,2,5], Joel N. Blankson[1], Stuart C. Ray[1], Sarah J. Wheelan[4], David L. Thomas[1], Ashwin Balagopal[1]*

Type 1 interferons (IFN) are critical for host control of HIV and simian immunodeficiency virus. However, it is unknown which of the hundreds of interferon-stimulated genes (ISGs) restrict HIV in vivo. We sequenced RNA from cells that support HIV replication (activated CD4$^+$ T cells) in 19 HIV-infected people before and after interferon-α2b (IFN-α2b) injection. IFN-α2b administration reduced plasma HIV RNA and induced mRNA expression in activated CD4$^+$ T cells: The IFN-α2b–induced change of each mRNA was compared to the change in plasma HIV RNA. Of 99 ISGs, 13 were associated in magnitude with plasma HIV RNA decline. In addition to well-known restriction factors among the 13 ISGs, two novel genes, CMPK2 and BCL-G, were identified and confirmed for their ability to restrict HIV in vitro: The effect of IFN on HIV restriction in culture was attenuated with RNA interference to CMPK2, and overexpression of BCL-G diminished HIV replication. These studies reveal novel antiviral molecules that are linked with IFN-mediated restriction of HIV in humans.

INTRODUCTION

Interferons are host defense cytokines that coordinate the expression of hundreds of cell-autonomous defense genes [(interferon-stimulated genes (ISGs)] to control viral infections in all vertebrates (*1*, *2*). Interferon-α2b (IFN-α2b), a quintessential type 1 interferon (IFN), has been used to treat chronic viral infections and has been tested in clinical trials against HIV. HIV-infected individuals treated with IFN experience a decline in the abundance of plasma viral RNA (*3*–*5*) and the number of cells harboring viral genomes (*6*). Sandler and colleagues, among others, have provided firm evidence that simian immunodeficiency virus (SIV) control by type 1 IFN requires induction of ISGs: They recently demonstrated that inhibition of type 1 IFN signaling in rhesus macaques reduced ISG induction and enhanced SIV replication and progression to AIDS (*7*–*9*). However, although it is clear that type 1 IFN exerts antiviral effects on HIV, SIV, and other viral infections, the molecular mechanisms and even the cells in which ISGs that restrict HIV in vivo are induced are largely unknown (*10*).

Several HIV restriction factors that are also ISGs have been described in CD4$^+$ T cells, including the apolipoprotein B mRNA-editing enzyme, catalytic polypeptide-like (APOBEC) gene family, MX2, IFITM1, and tetherin (*4*, *11*–*14*). Although their antiviral activities have been elegantly demonstrated in vitro, the in vivo effects of these genes on HIV in humans remain hard to quantify, partly because their expression in vivo is in the setting of broad immune activation that may be only partly driven by type 1 IFN signaling (*15*). We hypothesized that the antiviral effect of IFN-α2b on HIV in untreated people is due to ISG induction in activated CD4$^+$ T cells, the principal source of HIV in blood (*16*). Moreover, we reasoned that we could couple the natural variability in human ISG induction with the variable HIV response to IFN-α2b to identify the genes that are most likely to restrict HIV in vivo.

[1]Department of Medicine, Johns Hopkins University School of Medicine, Baltimore, MD 21205, USA. [2]Department of Molecular Biology and Genetics, Johns Hopkins University School of Medicine, Baltimore, MD 21205, USA. [3]Center for Computational Biology, Johns Hopkins University School of Medicine, Baltimore, MD 21205, USA. [4]Department of Oncology, Johns Hopkins University School of Medicine, Baltimore, MD 21287, USA. [5]Howard Hughes Medical Institute, Johns Hopkins University School of Medicine, Baltimore, MD 21205, USA.
*Corresponding author. Email: abalago1@jhmi.edu

RESULTS

IFN-induced restriction of HIV viremia in people is consistent with intracellular effects

We observed a 0.24 to 2.14 (median, 0.85) $\log_{10}$ copies/ml of decline in plasma HIV RNA at 1 week ($P = 0.003$) after administering a single weight-based injection of IFN-α2b to 19 untreated HIV and hepatitis C virus (HCV) coinfected persons (Fig. 1A and fig. S1A). We broadly considered two hypotheses that might explain the decline in HIV RNA after IFN-α2b administration. First, we hypothesized that HIV RNA decline resulted from the up-regulation of HIV restriction factors by IFN-α2b in susceptible and infected cells. Alternatively, we hypothesized that IFN-α2b may have diverse actions outside of susceptible and infected cells that include bone marrow suppression and changes to cellular immunity against HIV-infected cells (*17*–*19*). We adapted standard mathematical models of HIV kinetics after antiviral treatment to test these hypotheses. We considered an array of ISGs as putative antivirals (*17*–*20*), hypothesizing that they could either affect the first-order rate constant of target cell infection (β) or the rate of virus production in infected cells (k) (Fig. 1B). An example of an ISG that might affect β is MX2, which inhibits HIV preintegration, whereas an example of an ISG that affects k is tetherin (BST2), which prevents virus release (fig. S2). Alternatively, we modeled whether IFN-α2b–induced changes to the number of target cells (x) (for example, during bone marrow suppression) or loss of infected cells (y) (for example, by enhancing cellular immunity) might explain the observed plasma viral kinetics. The observed HIV kinetics after IFN-α2b administration were most consistent with models that incorporated IFN-α2b–induced effects on β and/or k and were least consistent with models of changes to x

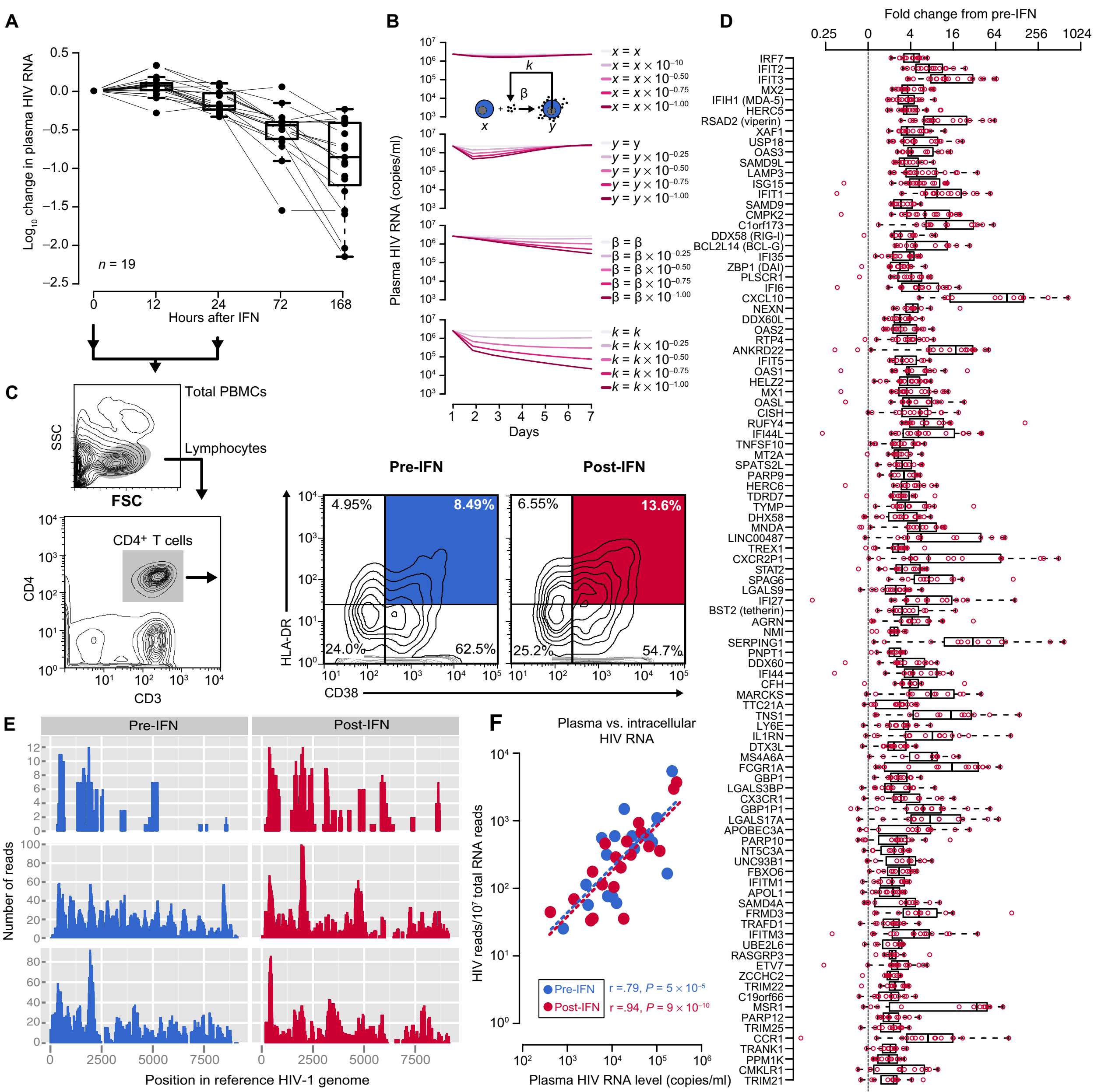

Fig. 1. Administration of pegylated IFN-α2b induces a decline in plasma HIV RNA and stimulates gene expression in activated CD4$^+$ T cells. (**A**) Observed HIV kinetics after IFN-α2b in 19 participants. Boxplots are shown with overlaid values of in vivo $\log_{10}$ copies/ml of changes in plasma HIV RNA from baseline among patients who received IFN-α2b. Lines indicate longitudinal measurements from the same individual. (**B**) Infections were first simulated for 1000 days using three standard differential equations $dx/dt = \lambda - dx - \beta xv$, $dy/dt = \beta xv - ay$, and $dv/dt = ky - uv$ (λ is the production rate of uninfected cells, x is the number of uninfected cells, d is the decay rate of uninfected cells, β is the first-order rate constant of infection, v is the plasma HIV RNA level, y is the number of infected cells, a is the decay rate of infected cells, k is the first-order rate constant of virus production in infected cells, and u is the first-order rate constant of virus decay; see fig. S2) using established starting values ($x = 10^6$, $y = 1$, $v = 10^5$, $\lambda = 10^5$, $d = 0.1$, $a = 0.5$, $\beta = 2 \times 10^{-7}$, $k = 100$, and $u = 5$). Resulting values were then used as input into the same equations, separately modifying the indicated variable by the indicated factor and run for 7 days to reflect observed data in (A). We assumed that the effect of IFN-α2b on plasma HIV RNA can be due to changes in the numbers of susceptible cell numbers (x), changes in susceptibility of those cells (β), changes in the numbers of infected cells (y), and changes in the release of virus from infected cells (k); therefore, we varied x, y, β, and k in the models. Whereas varying x and y had minimal effects on modeling HIV viremia, varying β and k had significant effects on HIV kinetics that mirrored the observed data in (A). (**C**) Representative flow cytometry data and sorting algorithm for isolation of activated CD4$^+$ T cells from total peripheral blood mononuclear cells (PBMCs) at baseline (Pre–IFN-α2b; blue) and 24 hours after injection with IFN-α2b (Post–IFN-α2b; red). SSC, side scatter. (**D**) Boxplots with overlaid points showing the fold changes for the 99 genes that significantly changed with IFN-α2b administration across the cohort, after adjustment for multiple comparisons. For each ISG, an individual point represents fold change data from a single person, and the boxplot represents summary fold change data across all people. (**E**) RNA sequencing (RNA-seq) reads from each person's activated CD4$^+$ T cells [CD3$^+$/CD4$^+$/CD38$^+$/HLA-DR$^+$; shown in (C)] were mapped and aligned to 2154 HIV reference genomes before and 24 hours after IFN-α2b. Displayed are representative alignment maps from three persons before and after IFN-α2b, demonstrating that the selection of these cells is adequate to testing how IFN-α2b restricts HIV replication. (**F**) RNA-seq reads from activated CD4$^+$ T cells that mapped to HIV correlated closely with plasma HIV RNA levels, confirming that infection of these cells is tightly associated with plasma viremia and viral kinetics in (A).

or y, which demonstrated transient or marginal effects on viremia (Fig. 1B).

IFN-α2b induces ISG expression in activated CD4$^+$ T cells

Next, we sought to empirically identify the factors responsible for the observed changes in viremia that we inferred were due to IFN-α2b–induced effects on β or k. We chose to investigate activated CD4$^+$ T cells, which comprise both susceptible cells (x) and infected cells (y). By using a more inclusive strategy, we avoided neglect of ISGs that could restrict either early events in the HIV replicative cycle (for example, entry and reverse transcriptions) or later events (for example, release). In other words, targeting only HIV-infected cells would have neglected ISGs that restrict HIV by preventing entry, uncoating, reverse transcription, or integration.

Activated CD4$^+$ T cells have been well described for their susceptibility to HIV and their contribution to plasma viremia (*20*–*22*). Although numerous phenotypic markers have been used to define activated CD4$^+$ T cells, we limited our phenotyping to two markers, CD38 and human leukocyte antigen–DR (HLA-DR), based on previous reports of HIV susceptibility, and to provide sufficient cells for sequencing. Several groups have reported that CD3$^+$/CD4$^+$/CD38$^+$/HLA-DR$^+$ T cells are enriched for HIV proviral DNA and HIV RNA (*20*–*22*). CD3$^+$/CD4$^+$/CD38$^+$/HLA-DR$^+$ cells were characterized and sorted before and after IFN-α2b by flow cytometry and fluorescence-activated cell sorting (FACS). Compared to pre–IFN-α2b, the percentage of CD4$^+$/CD38$^+$/HLA-DR$^+$ after IFN-α2b increased by a median [interquartile range (IQR)] of 5.4% (−1.6 to 6.9; $P = 0.02$) (Fig. 1C and fig. S3B). Flow cytometry allowed concomitant quantification of CD8$^+$ T cell activation, a well-defined marker of immune activation in HIV: CD8$^+$/CD38$^+$/HLA-DR$^+$ T cells increased by a median (IQR) of 19.1% (14.2 to 22.5; $P = 0.0001$) (fig. S3, A and C).

We reasoned that the intracellular factors that were responsible for IFN-α2b–induced HIV restriction would have to have been transcriptionally up-regulated 24 hours after IFN-α2b administration for their effects on viremia to have been apparent by 72 hours, as we observed in Fig. 1A. Therefore, we sequenced and quantified RNAs from purified populations of activated CD4$^+$ T cells before and 24 hours after IFN-α2b in the 19 persons, resulting in a total of 21,930 sequenced genes. Of these genes, 9631 met our prespecified criteria for being quantifiable in sufficient numbers of people to be evaluable across the cohort (see Materials and Methods). Among the 9631 genes, 99 were found to be up-regulated by IFN-α2b in vivo in activated CD4$^+$ T cells (Fig. 1D and fig. S4), supporting our decision to sequence RNAs at 24 hours. In contrast, we found no genes that were down-regulated. We further confirmed the appropriateness of our strategy of sequencing CD3$^+$/CD4$^+$/CD38$^+$/HLA-DR$^+$ T cells by mapping the RNA sequencing data to HIV reference sequences (see Materials and Methods). Intracellular HIV mRNA reads were readily identified in the sorted CD4$^+$/CD38$^+$/HLA-DR$^+$ T cells in most people and were closely associated with contemporaneous plasma HIV RNA levels (Fig. 1, E and F), supporting the selection of these cells as contributing to viremia.

The median magnitude of up-regulation across all 99 ISGs ranged from 2- to 92-fold, although there was considerable variability between individuals. The 99 ISGs included known HIV restriction factors such as MX2 and tetherin. In addition, several ISGs that have previously been implicated in viral immunity [RSAD2 (viperin), DDX58 (RIG-I), and IFITM3] were also identified, as were genes that have not been previously described as having antiviral roles [including, but not limited to, CMPK2 and BCL-G (BCL2L14)].

We sought to determine whether any of the 99 genes were newly identified as ISGs by querying the Interferome database v.2.01 (*23*). We found that CISH, LGALS17A, LINC00487, SPAG6, and TNS1 were induced in our samples and not annotated in the database. A review of the gene ontology in the database revealed that CISH and TNS1 have been previously implicated in immunity. A review of PubMed using these gene names as search terms revealed no publications for LGALS17A and LINC00487. SPAG6 is known to be required for flagella and cilia motility and in that capacity has been associated with increased susceptibility to otitis media (*24*); however, to our knowledge, there were no other reports of its role in immunity. We concluded that LGALS17A, LINC00487, and SPAG6 are novel ISGs.

We further characterized the ISGs that we identified by examining their transcriptional isoforms, exploiting the open-ended sequencing approach to the transcriptome where data were available. We examined five distinct transcript variants of MX2 (fig. S5): four of five (three coding and one noncoding) variants were significantly induced by IFN-α2b ($P < 0.05$ for all). Intriguingly, a noncoding variant of MX2 that contains the first exon and a partially spliced retained intron (uc002yze.1) was highly expressed. Examination of CMPK2 and BCL-G splice variants revealed a significant increase in the expression of all five and three detected isoforms, respectively, after IFN-α2b ($P < 0.05$ for each; fig. S6).

IFN-α2b induces ISGs in vivo that are associated with HIV restriction

We noted that the baseline abundance of ISGs before IFN-α2b, as quantified by the RNA-seq reads per gene (fragments per kilobase of transcript per million mapped reads; fig. S7), was not associated with baseline plasma HIV RNA, similar to the findings reported previously with a more restricted set of ISGs (*5*). We also found that a summary measure of ISG induction (quantified as the mean fold change in expression of all 99 ISGs) in each participant was only marginally associated with plasma HIV RNA decline ($P = 0.08$, $R = -0.41$; fig. S8). However, the marginal association supported the idea that a more refined analysis might reveal which among the 99 ISGs were potentially directly related to the observed decline in HIV viremia.

We extended this reasoning, hypothesizing that the magnitude of decline in viremia to IFN-α2b in vivo might follow a dose-response relationship with the ISG(s) that was directly responsible for HIV restriction, as has been shown previously for known HIV restriction factors (*4*). We compared the magnitude of increase in each of the 99 ISGs with the magnitude of plasma HIV RNA decline among the 19 individuals. In doing so, we identified 13 genes whose up-regulation in activated CD4$^+$ T cells 24 hours after IFN-α2b administration was closely correlated with subsequent plasma HIV RNA decline (Fig. 2A), supporting a potential causal role for these ISGs in HIV restriction. To control for false detection, we confirmed that the same algorithm failed to identify ISG induction in activated CD4$^+$ T cells that was associated with HCV RNA decline in the same people to the same level of significance as with HIV (Fig. 2B), which could also be inferred from the dissimilar HIV and HCV kinetics in the same people (fig. S1B).

Among the 13 candidate restriction factors, we found MX2, APOBEC3A, and IFITM1, all of which have been described as

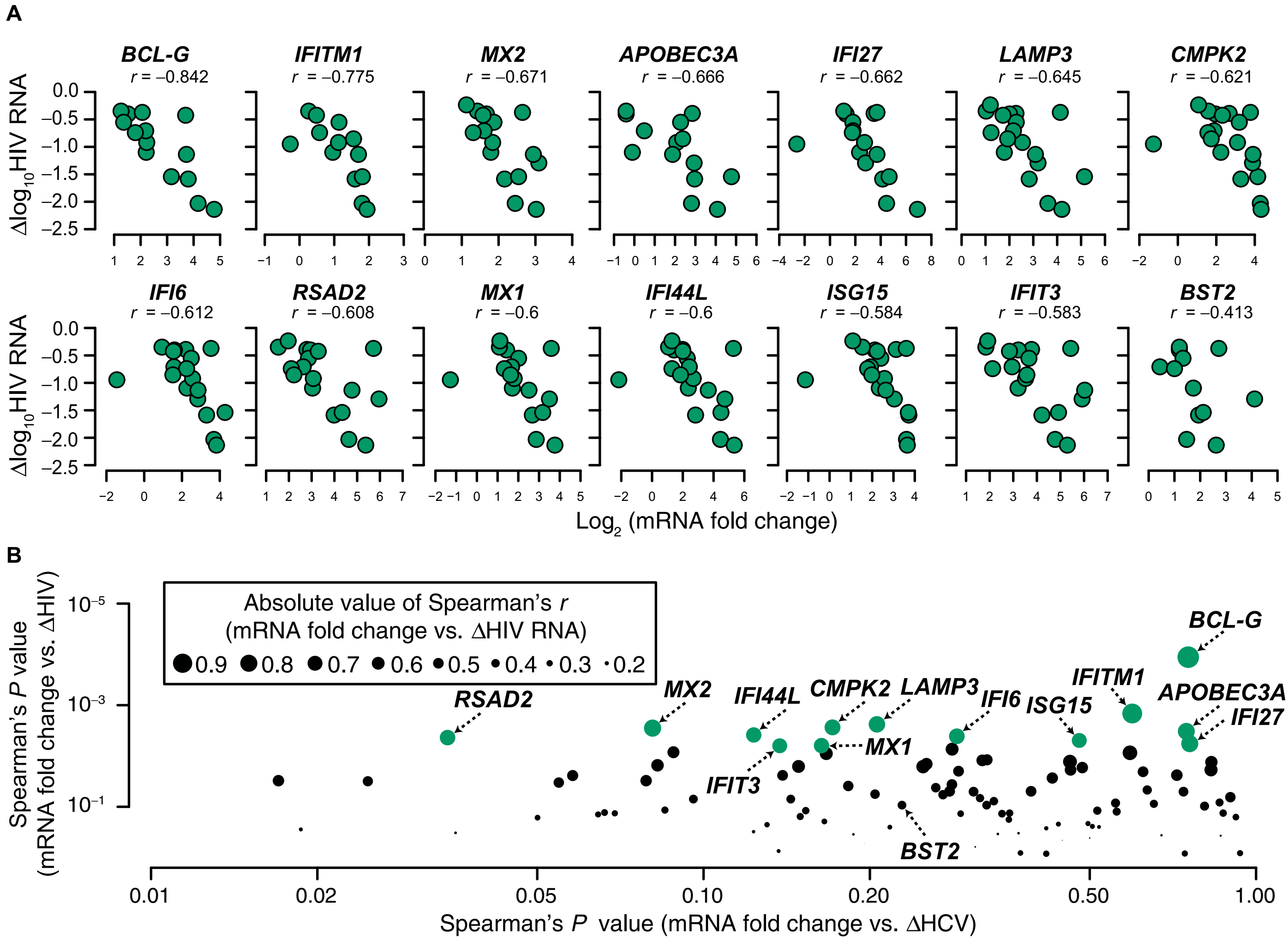

Fig. 2. Identification of ISGs that are putative interferon-induced HIV restriction factors in activated CD4⁺ T cells. (**A**) Individual scatterplots of 13 of 99 ISGs that were significantly correlated with plasma HIV RNA decline after IFN-α2b administration, adjusting for multiple comparisons. BST2, a known IFN-inducible HIV restriction factor, is also shown for reference. We assumed that the induction of an HIV restriction factor had to precede the change in plasma HIV RNA: Therefore, the fold change in mRNA expression of each gene in activated $CD4^+$ T cells after 24 hours of IFN-α2b is shown in the *x* axis, and the change in plasma HIV RNA level 1 week after IFN-α2b is shown the *y* axis. (**B**) Putative HIV restriction factors are not bystanders of IFN-α2b induction but appear to be specific for HIV. Each of the 99 ISGs identified in Fig. 1 is depicted by individual dots. The strength of the association of the induction of each ISG with plasma HIV RNA decline is shown as the Spearman's *P* value in the *y* axis and by the size of each dot (scaled to represent the Spearman's correlation coefficient). Genes that met statistical significance after adjustment for multiple comparisons are shown as green dots. To validate against false detection, Spearman correlations were also performed for the induction of the same genes and plasma HCV RNA decline (*P* values along the *x* axis), revealing no genes that were up-regulated in activated $CD4^+$ T cells were significantly associated with HCV, after the adjustment for multiple comparisons.

restricting HIV in vitro (*11*–*13*, *25*–*27*), confirming the validity of our strategy. Surprisingly, we did not find up-regulation of APOBEC3G or APOBEC3F. In addition to previously described restriction factors, several of the newly identified ISGs were also strongly associated with plasma HIV RNA decline, including CMPK2 and BCL-G (Fig. 2B).

We noticed that CMPK2, found on chromosome 2, is adjacent to and inverted with respect to RSAD2, a better characterized ISG with well-described antiviral activity (Fig. 3A). To understand whether CMPK2 mRNA up-regulation after IFN was incidental, as a bystander, given the possibility of a shared upstream coding region with RSAD2, we performed pairwise correlations of gene up-regulation among the 13 putative restriction factors and across the 19 people. We identified several groupings of shared gene expression, with two isolated genes (BCL-G and BST2) that did not share much gene expression with the other ISGs (Fig. 3B). We defined four distinct gene clusters by principal components analyses: CMPK2 up-regulation clustered more closely with MX1 than with MX2 or RSAD2 (Fig. 3A), while BCL-G and BST2 appeared to have their own independent expression patterns (Fig. 3, B and C). These results left open the possibility that CMPK2 and BCL-G inhibited HIV separately from each other and from other previously described restriction factors and were not incidentally found because of shared regulatory patterns with other restriction factors.

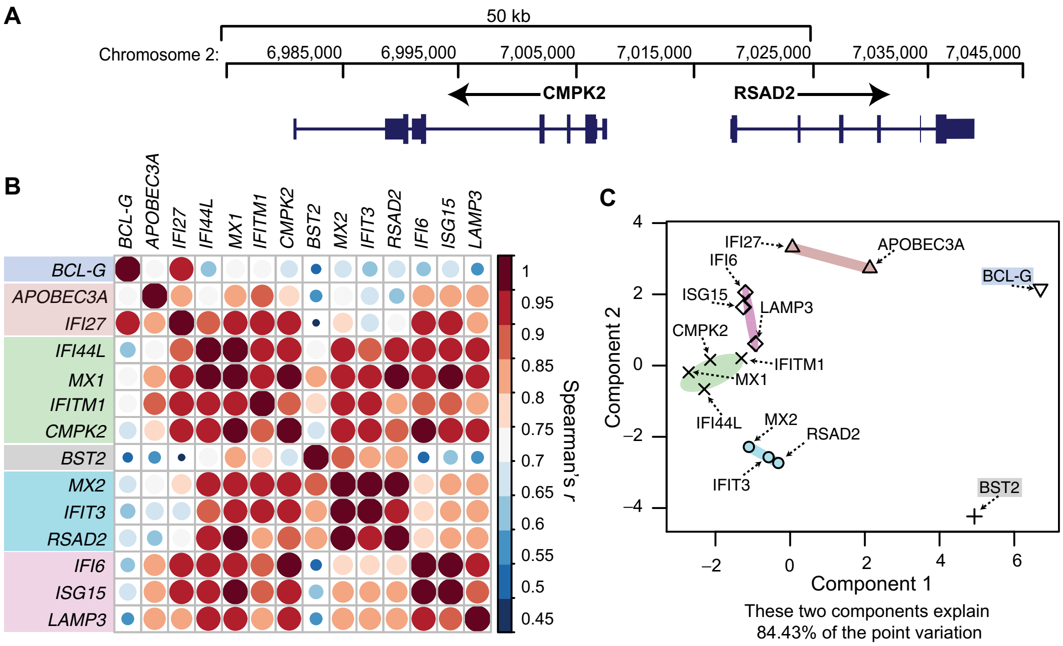

Fig. 3. Covariate analysis of ISG expression reveals distinct regulation of CMPK2 and RSAD2. (**A**) Genomic positions of CMPK2 and RSAD2, magnified on CMPK2, illustrate a shared upstream region for both genes. (**B**) Pairwise correlation plots of fold changes for the putative HIV restriction factors and BST2 as reference demonstrate different clusters of gene expression and distinct patterns of regulation. (**C**) *K*-means clustering of principal components analysis grouping all points into four clusters. The same color scheme used to demarcate clusters in (B) is used in (C). Despite their shared upstream region, CMPK2 and RSAD2 show distinct regulatory patterns. BCL-G appears to be regulated separately from other reported and novel HIV restriction factors.

IFN-mediated restriction of HIV depends on CMPK2 and BCL-G in vitro

We confirmed that IFN induced the putative HIV restriction factors CMPK2 and BCL-G in multiple cell lines over 24 hours (Fig. 4A). All isoforms of CMPK2 and BCL-G were up-regulated upon IFN treatment in most of the cell lines that were tested, although to different degrees. In addition, we confirmed that the major isoforms of CMPK2 and BCL-G were induced by IFN in primary cells: These genes were up-regulated in CD4$^+$ T cells from two healthy donors (HIV and HCV uninfected) who were activated ex vivo and stimulated with IFN for 24 hours (Fig. 4B). These in vitro data confirmed that CMPK2 and BCL-G are IFN-inducible.

Next, we identified cell lines in which IFN treatment resulted in the largest declines in HIV replication, indicating that they up-regulated the requisite ISGs for HIV restriction (fig. S9). We found that THP-1 cells and MT4 cells showed reductions of at least 1 $\log_{10}$ copies/ml of HIV when treated with IFN over a range of viral inocula, compared to untreated cells. These two cell lines were notable for also demonstrating the best induction of CMPK2 and BCL-G (Fig. 4A and fig. S10).

Because CMPK2 was robustly induced in THP-1 cells, we used RNA interference (RNAi) in THP-1 cells to confirm the restriction of HIV by CMPK2. Small interfering RNAs (siRNAs) to CMPK2 achieved maximum suppression of IFN-induced CMPK2 protein expression compared to cells transfected with scrambled control siRNAs (fig. S11A). Although the scrambled siRNAs appeared to induce expression of CMPK2 protein even in the absence of IFN, we found the same effect on MX2 expression (fig. S11B). Using this system, THP-1 cells were inoculated with the HIV-IIIB strain at decreasing concentrations after siRNA transfection and treated with either IFN or medium (Fig. 4C). The IFN-induced restriction of HIV was markedly attenuated in cells transfected with siRNAs against CMPK2 compared to cells transfected with scrambled siRNAs (Fig. 4C and fig. S12). The effect was approximately 10-fold and was observed over a wide range of HIV inocula. Notably, baseline HIV titers in the IFN-untreated cells were significantly greater in the scrambled siRNA-treated cells than in the siCMPK2-treated cells at several HIV inocula, further supporting a role of CMPK2 in HIV control (fig. S12).

We attempted to perform similar experiments to confirm the effect of BCL-G on HIV restriction in MT4 cells. However, we were unable to detect native BCL-G protein in MT4 cells using multiple Western blot antibodies, although we had no difficulty visualizing the protein when cloned into a plasmid and transfected into 293 T cells (fig. S13). Since 293T cells do not support HIV replication, we cloned BCL-G into a pMyc vector and transfected the myc–BCL-G plasmid into TZM-bl cells and MT4 cells. We also transfected a myc-MX2 construct and an empty myc construct into TZM-bl cells and MT4 cells as positive and negative controls, respectively. Using this strategy, we were able to visualize the myc–BCL-G in TZM-bl cells using an anti–BCL-G antibody (fig. S13), and this corresponded to the size seen in 293T cells. Probing with an anti-myc antibody revealed the protein as well, confirming its identity. myc-MX2 was similarly visualized in TZM-bl cells. However, transfection into MT4 cells or in a pCMV vector failed to reveal the genes consistently by Western blotting. Therefore, we transfected myc–BCL-G, myc-MX2, and an empty myc vector into TZM-bl cells and infected the cells with the HIV-IIIB strain over a range of inocula (Fig. 4D). Viral titers were measured after 48 hours. Compared to the empty myc vector, myc–BCL-G and myc-MX2 significantly reduced the production of HIV, as measured by luciferase activity. Collectively, we confirmed

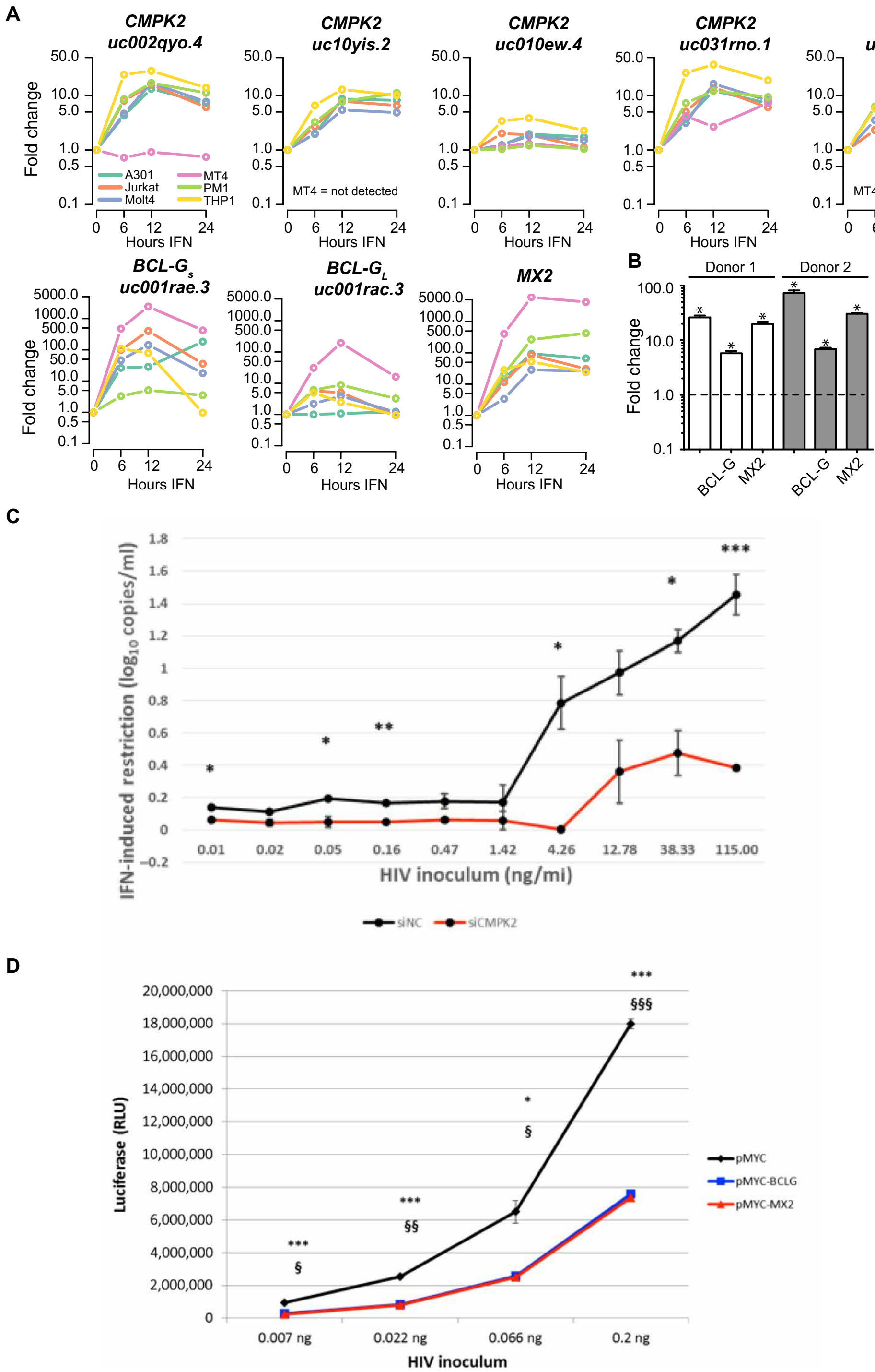

Fig. 4. Interferon-induced HIV restriction in vitro is dependent on CMPK2 and BCL-G. (**A**) IFN induces CMPK2 and BCL-G in multiple cell lines. Real-time quantitative polymerase chain reaction (qPCR) data showing the up-regulation of CMPK2, BCL-G, and MX2 (as a positive control) in response to IFN in six cell lines at 0, 6, 12, and 24 hours. (**B**) CMPK2 and BCL-G are ISGs in primary cells. Real-time qPCR data of CMPK2, BCL-G, and MX2 in response to IFN in activated $CD4^+$ T cells ex vivo from two healthy donors who were not infected with HIV or HCV. (**C**) CMPK2 knockdown diminishes HIV restriction of HIV. CMPK2 knockdown was performed using pooled siRNAs in THP-1 cells (red) and compared to a scrambled siRNA (black). Cells were then inoculated with a wide range of HIV inocula (*x* axis) and split and either treated with IFN or left untreated. HIV replication was quantified by the TZM-bl luciferase assay. The log-transformed difference in HIV replication between IFN-treated and IFN-untreated cells for each condition is shown in the *y* axis. *$P < 0.05$; **$P < 0.01$; ***$P < 0.005$. (**D**) BCL-G inhibits HIV production. myc-tagged BCL-G, myc-tagged MX2, and an empty pMyc vector were transfected into TZM-bl cells. Cells were inoculated with a wide range of HIV inocula (*x* axis). HIV replication was quantified by the TZM-bl luciferase assay. The raw luciferase values, after the adjustment for baseline differences, are shown. Statistical significance in differences in luciferase activity between myc–BCL-G transfected cells and myc control cells are denoted by *$P < 0.05$; **$P < 0.01$; ***$P < 0.005$. Statistical significance in differences in luciferase activity between myc-MX2–transfected cells and myc control cells are denoted by $^{§}P < 0.05$; $^{§§}P < 0.01$; and $^{§§§}P < 0.005$.

that HIV restriction by IFN is associated with CMPK2 and BCL-G, genes that were identified because (i) they were up-regulated in activated $CD4^+$ T cells in HIV-infected people who received exogenous IFN-α2b, and (ii) the magnitude of their up-regulation corresponded with the observed decline in plasma HIV RNA levels.

DISCUSSION

By sequencing mRNAs in the principal cells in which HIV replicates, and by measuring the differences in their induction against differences in the reduction of plasma HIV RNA, we have identified CMPK2 and BCL-G as being associated with IFN-α2b–induced HIV restriction. We also show, for the first time, that the recently described HIV restriction factor MX2 restrained HIV replication in vivo, albeit to different degrees among the 19 people. We and others have shown that differences in the transcriptional program of a cell type affect its susceptibility to HIV and its IFN sensitivity (*28–31*). To our knowledge, ours is the first in vivo study that has focused on the discovery of novel HIV restriction factors in activated $CD4^+$ T cells from infected persons (*7*). Our findings underscore that, despite the remarkable diversity of the IFN transcriptional program, a specific set of ISGs have direct antiretroviral roles. Accordingly, the results may suggest new approaches to the control of chronic HIV infection.

CMPK2 has been annotated as an ISG before, but its antiviral activity has been unclear. Its genomic location on chromosome 2 is nestled between *RSAD2* and the newly described negative regulator of the interferon response (NRIR), an interferon-induced long noncoding RNA that is a negative regulator of IFN responses (*32*). Hence, *CMPK2* sits in a transcriptionally active hotspot for IFN regulation. CMPK2 catalyzes the phosphorylation of deoxyuridine monophosphate (dUMP) (*33*), an intermediate step in the overall conversion of dUMP to deoxyuridine triphosphate (dUTP). Uracilation of retroviral genomes has been recently reported to be a novel mechanism of HIV restriction that is dependent on high intracellular levels of dUTP (*34*). Although it is possible that IFN-inducible CMPK2 permits uracilation of retroviral genomes, further experimental evidence is required to confirm this role of CMPK2.

The function of BCL-G remains poorly understood. There is controversy as to whether BCL-G is involved in apoptosis (*35*, *36*). Its "BCL" nomenclature derives from its BH2 and BH3 domains. Overexpression of BCL-G significantly limited HIV production to a level similar to what was observed with MX2. However, given the technical difficulties in visualizing native BCL-G, it will be important to demonstrate its efficacy as an HIV restriction factor in a more representative model to fully characterize whether it involves other members of the BCL family and whether apoptosis is involved.

We encountered several challenges in this investigation. We selected $CD4^+$ T cell markers that corresponded well with HIV-infected or HIV-susceptible cells. We used CD38 and HLA-DR double positivity to identify activated $CD4^+$ T cells based on extensive previous reports underscoring that these cells are among the most susceptible to HIV (*20–22*). However, it is possible that other sorting strategies could have also been used. We identified HIV mRNA in sorted $CD3^+/CD4^+/CD38^+/HLA\text{-}DR^+$ cells, which at least guaranteed that a portion of our sorted cells was HIV-infected. We reasoned that had we strictly focused on only HIV-infected cells, we would have omitted the effects of IFN-α2b on preventing infection of target, uninfected cells, which translates mathematically to the β first-order rate constant of HIV infectivity (Fig. 1B and fig. S2). In other words, we may have missed genes that are most active against HIV in uninfected but susceptible cells, such as MX2, APOBEC3A, and IFITM1. Another potential challenge is that we designed our study to identify HIV restriction factors whose mRNA transcription was inducible with IFN-α2b in activated $CD4^+$ T cells; therefore, we would not have been able to identify constitutively expressed restriction factors that endured IFN-α2b–induced posttranslational modifications, nor could we identify factors in other cells (such as natural killer cells or $CD8^+$ T cells) that might lead to improved immunologic targeting of HIV-infected cells. Finally, we used pegylated IFN-α2b to induce ISG expression; it is possible and even likely that other type 1 interferons could have induced a distinct set of genes that restricted HIV by other mechanisms, as recently suggested by Harper *et al.* (*37*). However, that consideration does not detract from our confidence in revealing the mechanism through which interferon-α, the most common therapeutic interferon, constrains HIV. It is also not clear how CMPK2 and BCL-G relate to previously described ISG restriction factors in vivo, such as APOBEC3G, tetherin, and SAMHD1, although our data provide some clues into patterns of co-regulation.

Here, we have provided in vivo and in vitro evidence that suggest that CMPK2 and BCL-G are two novel putative IFN-induced HIV restriction factors. HIV restriction highlights the ongoing battle between virus and host, reveals potential roadblocks in the HIV life cycle, and may provide novel therapeutic targets for HIV control. The actions of CMPK2 and BCL-G do not appear to be related and bespeak of the broad antiviral actions of type 1 IFN. In addition, CMPK2 and BCL-G showed markedly different amounts of up-regulation among the people in our study, suggesting genetic differences in their induction and HIV restriction. Future studies should focus on understanding the magnitude of adaptive pressure that CMPK2 and BCL-G impose on HIV, since resistance to antiviral factors is perhaps the best measure of their relevance. Further research will also be required to test whether CMPK2 or BCL-G can be exploited to cure patients with HIV.

MATERIALS AND METHODS

Human subjects

The primary outcome of the study was to compare gene expression in activated $CD4^+$ T cells with HIV RNA changes in plasma following administration of IFN-α2b (ΔHIV_{IFN}): 20 persons with HIV-HCV coinfection were enrolled in a prospective study of HIV and HCV viral kinetics before antiretroviral therapy (ART) (*38*). One of the 20 participants did not complete the study. Because complete HIV viral kinetic measurements were not available for this participant, the individual was excluded from the final analysis. Persons with chronic HIV and HCV infections were recruited from the Johns Hopkins HIV Clinic, the Baltimore City Sexually Transmitted Diseases Clinic, and other area clinics. HIV infection was established by detection of HIV antibodies and an HIV RNA level of >400 copies/ml; chronic HCV infection was determined by detection of HCV antibodies and an HCV RNA level of >100,000 IU/ml for >6 months. Subjects had received <24 months of ART over their entire lives and none within 6 months. Subjects were also excluded if hepatitis B surface antigen (HBsAg) was detected in plasma; they were pregnant; there was a history of severe depression or any uncontrolled disease; platelet count was <50,000/mm^3; and there was a contraindication to use of raltegravir, tenofovir disoproxil fumarate, or emtricitabine. Because therapy was judged too urgent to wait for study procedures as per current treatment guidelines for HIV and HCV, persons at screening whose CD4$^+$ T lymphocyte counts were <200/mm^3 or who had cirrhosis were excluded. A total of 32 patients were screened to identify 20 study subjects (table S1): 1 of 20 subjects did not complete the study. Subjects were admitted to the Johns Hopkins Hospital Clinical Research Unit. A single injection of pegylated IFN-α2b (1.5 μg/kg) was administered subcutaneously. Thereafter, blood was collected every 6 hours, and the patient was discharged 24 hours after the IFN-α2b dose. The patient returned 48 hours, 72 hours, 7 days, and 14 days after the IFN-α2b dose for plasma HIV RNA measurements. All subjects gave written informed consent to the protocol. The Johns Hopkins University School of Medicine Institutional Review Board approved this study.

Modeling the contributions of various features of HIV infection

The three differential equations $dx/dt = \lambda - dx - \beta xv$, $dy/dt = \beta xv - ay$, and $dv/dt = ky - uv$ (λ is the production rate of uninfected cells, x is the number of uninfected cells, d is the decay rate of uninfected cells, β is the first-order rate constant of infection, v is the plasma viral load, y is the number of infected cells, a is the decay rate of infected cells, k is the first-order rate constant of virus production in infected cells, and u is the first-order rate constant of virus decay) were integrated using "integrateODE" function in the "mosaic" package version 0.9.2-2 in R (www.r-project.org) version 3.1.2 for 1000 days using standard starting values ($x = 1 \times 10^6$, $y = 1$, $v = 100{,}000$, $\lambda = 1 \times 10^5$, $d = 0.1$, $a = 0.5$, $\beta = 2 \times 10^{-7}$, $k = 100$, and $u = 5$) (*19*, *39*, *40*). The solution values were then used as input into another integration but varying either x, β, k, or a by the indicated factor and run to simulate an additional 3 weeks (300 days for a) with these newly imposed values.

Laboratory testing

Unless otherwise indicated, all laboratory testing of study participants was performed in the clinical laboratory of the Johns Hopkins Hospital.

Viral RNA testing

To reduce interassay variance, HCV and HIV RNA testing for a given subject were done at the same time on plasma centrifuged within 30 min of collection and stored at −20°C for up to 25 hours and then at −80°C until testing. HIV RNA testing was done using the Abbott RealTime HIV Assay (no. 02631-090). HCV RNA testing was done using the Abbott RealTime HCV Amplification Reagent Kit (no. 04J86-90). To provide information in "real time," such as for screening into the study, additional HCV RNA tests were performed by the commercial laboratory of the Johns Hopkins Hospital using the Roche COBAS AmpliPrep/COBAS TaqMan HCV Test v. 1.0. Although both were reported in international units, analyses were primarily done on results from one or the other laboratory. CD4$^+$ T cell count was measured by flow cytometry of whole blood that was delivered to the Johns Hopkins Hospital clinical laboratory.

Isolation of activated CD4$^+$ T cells

Previously frozen PBMCs from only before and 24 hours after IFN-α2b (*38*) were thawed, washed, and incubated with CD3-FITC (BioLegend), CD4-PE/Cy7 (BioLegend), CD8-APC (BD Biosciences), HLA-DR–PE (BioLegend), and CD38-BV421 (BioLegend) antibodies for 40 min at 4°C as per the manufacturers' recommendation. Immediately before sorting, plasma membrane–compromised cells were labeled with propidium iodide (Sigma-Aldrich). FACS was performed on a MoFlo Legacy Sorter (Beckman Coulter) at the Johns Hopkins School of Public Health Flow Cytometry Core Facility. The population of interest was sorted directly into ≥4 volumes of Quick-RNA MicroPrep lysis buffer (Zymo Research) as per the manufacturer's recommendation. Sorting was stopped when the number of sorted cells reached 125,000 cells, although many samples did not reach this number. Flow cytometry analysis on two randomly selected post-sort samples revealed >95% purity. Sorted samples were vortexed, incubated for 10 min at room temperature, vortexed again, and frozen at −80°C until isolation.

Activated CD4$^+$ T cell RNA isolation

Isolation was performed using the Quick-RNA MicroPrep kit (Zymo Research) according to the manufacturer's protocol without the on-column deoxyribonuclease (DNase) treatment. The eluate was treated with DNAse I (Qiagen), then purified, and concentrated using the RNA Clean-up and Concentrator kit (Zymo Research) according to the manufacturer's protocol. The high-sensitivity assay for RNA or DNA was performed on RNA isolations and complementary DNA (cDNA) libraries, respectively, using a 2100 Bioanalyzer (Agilent).

Library preparation and sequencing

cDNA libraries were produced using the Ovation Single-cell RNA-seq kit (NuGEN) according to the manufacturer's specifications. Briefly, reverse transcription was carried out using a random hexamer to oligo-dT ratio of 50:1, and unique barcodes for each individual's samples were ligated to ~250–base pair enzymatically fragmented molecules. All samples were linearly amplified with 19 cycles of PCR using primer-annealing sites contained within the adapters. All sequencing was performed on a HiSeq 2500 (Illumina) at the Johns Hopkins Genetics Research Core Facility. All sequencing data were deposited in the National Center for Biotechnology Information (NCBI) Sequence Read Archive (accession number SRP068424).

Sequence mapping and differential expression calculation

Reads were aligned to the hg19 reference genome and annotated transcripts with RNA-Seq by Expectation Maximization (RSEM) (version 1.2.9) (*41*). Differential expression of genes and isoforms was calculated using EBSeq (version 1.11.0) (*42*), an empirical Bayesian hierarchical model for expression analysis of RNA-seq data (table S2 and fig. S4). Sashimi plots were produced in Integrative Genomics Viewer v2.3 using the same representative subject's data before and 24 hours after IFN-α2b. All sequence mapping and differential expression calculation were performed at the Johns Hopkins University Sidney Kimmel Comprehensive Cancer Center Next Generation Sequencing core.

Statistical analyses

Comparison values, including post-correction fold change, post-correction probability of differential expression (PPDE), and post-correction probability of equal expression (PPEE) values, were further analyzed in using "stats" in R version 3.1.2. Measurements for which neither the PPDE nor PPEE were ≥0.95 were discarded. In the determination of significance of a gene's change across the cohort, all fold-change calculations with PPEE value of ≥0.95 were set to 0. If there were remaining measurements for a gene in >10 of the individuals, a two-sided one-sample *t* test was performed on $\log_2$-transformed fold-change values. The resulting *P* values were adjusted for multiple comparisons using the Benjamini-Hochberg method (*43*). Genes with adjusted $P \leq 0.05$ for their fold-change were considered ISGs. Genes were determined to be previously annotated ISGs using "Interferome" v2.01 (*23*). Many filters can be imposed on this data set, and we chose to use a fairly liberal one: only limiting the database to any genes found in experiments using type 1 interferons in any cell type or organism with no false discovery rate imposed. This resulted in 3165 experimentally derived ISGs in humans and 3212 in mice. A liberal filter was chosen because more detailed filters on the data set reduced the sensitivity to identify previously annotated ISGs and almost uniformly failed to identify well-known ISGs in the literature (for example, IRF7).

Spearman's rank correlations were performed between ISG fold changes and plasma HIV RNA decline at 1 week after IFN-α2b injection (with fold-changes with PPEE values of ≥0.95 retained as their posterior fold-change values). Pairwise correlation plots were constructed using "corrplot" (version 0.73). The *K*-means clustering was performed using "cluster" (version 1.15.3), with the number of clusters set to 4 to best illustrate the grouping of genes by their induction pattern and plotted using cluster (version 2.0.4). Wilcoxon rank sum tests were performed on untransformed data in discovery analyses unless indicated otherwise. Two-sample unpaired one-way *t* tests were performed in cell culture studies, as these experiments were performed to validate observations previously made in vivo.

In vitro IFN treatments

Six cell lines THP-1, MT4, MOLT4, A3.01, PM1, and Jurkat cells [National Institutes of Health (NIH) AIDS Reagent Bank] were treated with type 1 IFN (1000 U/ml) for 0, 6, 12, and 24 hours, and RNA was isolated using the Quick-RNA MicroPrep kit (Zymo Research). Reverse transcription was performed with SuperScript III (Invitrogen) according to the manufacturer's protocol using oligo-dT primers only. qPCR was performed using LightCycler SYBR Green Master Mix (Bio-Rad) according to the manufacturer and run on the LightCycler 480 (Bio-Rad) according to the manufacturer's protocol (primer sequences are listed in table S3). Fold-changes are in reference to untreated samples and normalized to the geometric mean of C_t (cycle threshold) values from RPL13A (Integrated DNA Technologies Assay ID: Hs.PT.58.47294843), RPL37 (Integrated DNA Technologies Assay ID: Hs.PT.58.20168410), and β actin (Integrated DNA Technologies Assay ID: Hs.PT.56a.40703009.g).

Ex vivo IFN treatments

PBMCs from two healthy platelet donors from the Johns Hopkins Transfusion Center were isolated and frozen as previously described. Thawed cells were cultured in 10% fetal bovine serum (FBS) RPMI containing interleukin-2 (1.6 ng/ml) and phytohemagglutinin (1 μg/ml) for 3 days, after which $CD4^+$ T cells were magnetically separated using an antibody-based negative selection $CD4^+$ T cell separation kit (Miltenyi). For each donor, duplicate 24-hour treatments with IFN (0 or 1000 U/ml) were performed. To adjust for differences in cell growth, the same number of counted cells was isolated from each condition using the RNeasy Plus RNA isolation kit (Qiagen) according to the manufacturer's protocol. Reverse transcription was performed using SuperScript III (Invitrogen) according to the manufacturer's protocol. qPCR was performed using LightCycler SYBR Green Master Mix (Bio-Rad) according to the manufacturer and run on the LightCycler 480 (Bio-Rad) according to the manufacturer's protocol (primer sequences are listed in table S3). Primers for uc002qyo.4 were used for CMPK2, and primers for uc001rac.3 were used for BCL-G. Fold-changes are shown in reference to samples treated with IFN (0 U/ml) and normalized to the geometric mean of C_t values from RPL13A (Integrated DNA Technologies Assay ID: Hs.PT.58.47294843), RPLP0 (Integrated DNA Technologies Assay ID: Hs.PT.58.20222060), and HPRT1 (Integrated DNA Technologies Assay ID: Hs.PT.58v.45621572).

Virus preparation

The full-length HIV-IIIB or pNL4.3 Δenv (mock) plasmids were transfected into 293T cells, and supernatants were spinoculated onto PM1 cells (NIH AIDS Reagent Bank) for 2 hours at 1200*g*. Cells were then incubated at 37°C for 10 days. Supernatants were passed through 0.22-μm filter, and virus was pelleted through a 20% sucrose layer for 2 hours at 150,000*g*. Pellets were resuspended in RPMI containing 10% FBS and stored at −80°C. Virus concentration was determined using the 96-well format Alliance HIV-1 P24 Antigen ELISA kit (PerkinElmer) according to the manufacturer's protocol.

Testing cell lines for their IFN-mediated restriction potential for HIV

The indicated nine cell lines (NIH AIDS Reagent Bank) were centrifuge-inoculated with varying amounts of HIV-IIIB. For each inoculum concentration, 200,000 cells were centrifuge-inoculated with 50 μl of RPMI containing 10% FBS at 1200*g* for 2 hours. Cells were allowed to rest for 24 hours at 37°C, and then each inoculum was split into two wells, one that received no treatment while the other received IFN (1000 U/ml). Both wells were incubated for an additional 72 hours at 37°C before supernatants were collected, and p24 measurements were performed.

In vitro RNAi, infection, IFN treatment, and measurement of HIV production

THP-1 cells were transfected with SMARTpool siGENOME siRNAs (Dharmacon) negative controls or siRNAs at 20 μM against CMPK2 using MACSfectin according to the manufacturer's protocol. Cells were rested in recovery media (20% FBS) at 37°C for 24 hours and were centrifuge-inoculated with purified replication-competent HIV-IIIB in threefold serial dilutions starting at 115 ng/μl in 50 μl of 10% FBS RPMI at 1200*g* for 2 hours. After washing twice with media, cells were rested for 24 hours at 37°C, and duplicates of virus-inoculated cells was left untreated and supplemented with 100 μl of media, while another set of duplicates of virus-inoculated cells was treated with IFN (1000 U/ml). After 48 hours of IFN treatment, supernatants were removed, and 100 μl of this dilution was transferred to 10,000 TZM-bl cells (NIH AIDS Reagent Bank) in 100 μl of Dulbecco's modified Eagle's medium (DMEM) containing 10% FBS and DEAE (20 μg/ml) and incubated at 37°C for 48 hours. Cells were washed with phosphate-buffered saline (PBS) and assayed for luciferase activity using the Luciferase Assay Kit (Promega). Log_{10} HIV inhibition was calculated by log-transforming the luciferase readings from the IFN-treated wells and subtracting these from the log-transformed luciferase readings from the untreated cells.

In vitro overexpression of BCL-G and MX2

BCL-G (HsCD00336098; www.ncbi.nlm.nih.gov/nucleotide/23271333) and MX2 (HsCD00335381; www.ncbi.nlm.nih.gov/nucleotide/23271333) cDNAs were obtained from the Harvard Medical School PlasmID repository. We then amplified BCL-G using the forward primer (5′-TATATAGGTACCATGTGTAGCACCAGTGGGT-3′) and the reverse primer (5′-AAGCAGGCGGCCGCTCAGTCTACTTCTT-CATGTGATATCCCA-3′), in conjunction with the Platinum Taq High Fidelity PCR system generating KPN1 and NOT1 restriction sites, respectively. Similarly, we amplified MX2 using the forward primer (5′-TGAGTAGGTACCATGTCTAAGGCCCACAAGCC-3′) and the reverse primer (5′-AAGCAGGCGGCCGCTCAGTGGAT-CTCTTTGCTGGAG-3′), in conjunction with the Platinum Taq High Fidelity PCR system generating KPN1 and NOT1 restriction sites, respectively. For both MX2 and BCL-G, we performed agarose gel electrophoresis and purified the resulting PCR products using the NucleoSpin Gel Extraction Kit (Macherey-Nagel), and sequences were verified using Sanger sequencing. Inserts and the pCMV-Myc-N DNA plasmid (Clontech) were digested simultaneously using KPN1 (New England Biolabs) and NOT1 (New England Biolabs) according to the manufacturer's protocol, purified using the NucleoSpin PCR Clean-up kit (Macherey-Nagel) according to the manufacturer's protocol, and ligated using the Quick Ligation system (New England Biolabs) according to the manufacturer's protocol. We then transformed TOP10 One Shot (Invitrogen) cells with the resulting ligation according to the manufacturer's protocol. We then obtained single colony plasmid sequences using the NucleoSpin Plasmid Mini Prep Kit (Macherey-Nagel) according to the manufacturer's protocol, and sequences were verified using Sanger sequencing using the pCMV Fw sequencing primer. We performed all Sanger sequencing at the Johns Hopkins Synthesis and Sequencing Facility. The resulting myc–BCL-G, myc-MX2, and empty pCMV-Myc-N (empty myc) vectors were transfected into TZM-bl cells using the PolyFect reagent (Qiagen) in 96-well plates for inoculation according to the manufacturer's protocol for HeLa cells. In parallel, six-well plates were transfected for protein analysis using Western blot. We generated lysates from the six-well plates 48 hours after transfection using the Promega 5× luciferase cell culture lysis buffer and ran SDS–polyacrylamide gel electrophoresis using the Novex system according to the manufacturer's protocol. HIV-IIIB was added to the cells 48 hours after transfection at 0, 0.007, 0.066, and 0.2 ng/ml p24 using D10 DMEM with DEAE-Dextran and hydrochloride (Sigma-Aldrich). Cell supernatants were collected, and cells were rinsed using 1× PBS. Promega cell lysis solution (1×) was prepared, and 50 μl was dispensed on cells for 10 min. Lysed cells (40 μl) were removed and transferred to a Costar 96-well white, flat-bottom plate for luciferase reading. Western blots were blocked using 3% bovine serum albumin (Sigma-Aldrich) in tris-buffered saline/0.1% Tween 20 at room temperature for 1 hour. Primary antibody myc 9E10 (1:10,000; 11667203001, Roche) was incubated overnight at 4°C.

SUPPLEMENTARY MATERIALS

Supplementary material for this article is available at http://advances.sciencemag.org/cgi/content/full/4/8/eaat0843/DC1

Fig. S1. Antiviral kinetics for HIV and HCV vary independently by person.

Fig. S2. Standard virologic models highlight different possible actions of ISGs on HIV replication.

Fig. S3. IFN-α2b administration results in changes in the proportion of activated $CD4^+$ and $CD8^+$ T cells.

Fig. S4. Approach to quantifying and identifying ISGs in RNAs from longitudinally sampled cells.

Fig. S5. IFN-α2b induces multiple MX2 isoforms in vivo.

Fig. S6. IFN-α2b induces multiple isoforms of CMPK2 and BCL-G.

Fig. S7. Baseline gene expression is not associated with plasma HIV RNA levels.

Fig. S8. Mean ISG induction and plasma HIV RNA decline.

Fig. S9. Interferon-mediated inhibition of HIV in vitro in multiple cell lines.

Fig. S10. CMPK2 and MX2 are induced by IFN in THP-1 cells.

Fig. S11. Knockdown of CMPK2.

Fig. S12. IFN restriction of HIV is dependent on CMPK2 in THP-1 cells.

Fig. S13. Expression of myc-tagged BCL-G and MX2 in vitro.

Table S1. Participant characteristics.

Table S2. RNA-seq metadata.

Table S3. qPCR primer sequences and amplicon location by exon.

REFERENCES AND NOTES

1. C. Langevin, E. Aleksejeva, G. Passoni, N. Palha, J.-P. Levraud, P. Boudinot, The antiviral innate immune response in fish: Evolution and conservation of the IFN system. *J. Mol. Biol.* **425**, 4904–4920 (2013).
2. J. D. MacMicking, Interferon-inducible effector mechanisms in cell-autonomous immunity. *Nat. Rev. Immunol.* **12**, 367–382 (2012).
3. D. M. Asmuth, R. L. Murphy, S. L. Rosenkranz, J. J. L. Lertora, S. Kottilil, Y. Cramer, E. S. Chan, R. T. Schooley, C. R. Rinaldo, N. Thielman, X.-D. Li, S. M. Wahl, J. Shore, J. Janik, R. A. Lempicki, Y. Simpson, R. B. Pollard, Safety, tolerability, and mechanisms of antiretroviral activity of pegylated interferon Alfa-2a in HIV-1-monoinfected participants: A phase II clinical trial. *J. Infect. Dis.* **201**, 1686–1696 (2010).
4. S. K. Pillai, M. Abdel-Mohsen, J. Guatelli, M. Skasko, A. Monto, K. Fujimoto, S. Yukl, W. C. Greene, H. Kovari, A. Rauch, J. Fellay, M. Battegay, B. Hirschel, A. Witteck, E. Bernasconi, B. Ledergerber, H. F. Günthard, J. K. Wong; Swiss HIV Cohort Study, Role of retroviral restriction factors in the interferon-α–mediated suppression of HIV-1 in vivo. *Proc. Natl. Acad. Sci. U.S.A.* **109**, 3035–3040 (2012).
5. A. Katsounas, A. C. Frank, R. A. Lempicki, M. A. Polis, D. M. Asmuth, S. Kottilil, Differential specificity of interferon-alpha inducible gene expression in association with human immunodeficiency virus and hepatitis C virus levels and declines in vivo. *J. AIDS Clin. Res.* **6**, 1000410 (2015).
6. L. Azzoni, A. S. Foulkes, E. Papasavvas, A. M. Mexas, K. M. Lynn, K. Mounzer, P. Tebas, J. M. Jacobson, I. Frank, M. P. Busch, S. G. Deeks, M. Carrington, U. O'Doherty, J. Kostman, L. J. Montaner, Pegylated interferon alfa-2a monotherapy results in suppression of HIV type 1 replication and decreased cell-associated HIV DNA integration. *J. Infect. Dis.* **207**, 213–222 (2013).
7. J. W. Schoggins, S. J. Wilson, M. Panis, M. Y. Murphy, C. T. Jones, P. Bieniasz, C. M. Rice, A diverse range of gene products are effectors of the type I interferon antiviral response. *Nature* **472**, 481–485 (2011).
8. M. Abdel-Mohsen, X. Deng, T. Liegler, J. C. Guatelli, M. S. Salama, H. E.-d. A. Ghanem, A. Rauch, B. Ledergerber, S. G. Deeks, H. F. Günthard, J. K. Wong, S. K. Pillai, Effects of alpha interferon treatment on intrinsic anti-HIV-1 immunity in vivo. *J. Virol.* **88**, 763–767 (2014).
9. N. G. Sandler, S. E. Bosinger, J. D. Estes, R. T. R. Zhu, G. K. Tharp, E. Boritz, D. Levin, S. Wijeyesinghe, K. N. Makamdop, G. Q. del Prete, B. J. Hill, J. K. Timmer, E. Reiss, G. Yarden, S. Darko, E. Contijoch, J. P. Todd, G. Silvestri, M. Nason, R. B. Norgren Jr., B. F. Keele, S. Rao, J. A. Langer, J. D. Lifson, G. Schreiber, D. C. Douek, Type I interferon responses in rhesus macaques prevent SIV infection and slow disease progression. *Nature* **511**, 601–605 (2014).
10. J. W. Schoggins, C. M. Rice, Interferon-stimulated genes and their antiviral effector functions. *Curr. Opin. Virol.* **1**, 519–525 (2011).
11. C. Goujon, O. Moncorgé, H. Bauby, T. Doyle, C. C. Ward, T. Schaller, S. Hué, W. S. Barclay, R. Schulz, M. H. Malim, Human MX2 is an interferon-induced post-entry inhibitor of HIV-1 infection. *Nature* **502**, 559–562 (2013).
12. J. Lu, Q. Pan, L. Rong, S.-L. Liu, C. Liang, The IFITM proteins inhibit HIV-1 infection. *J. Virol.* **85**, 2126–2137 (2011).
13. M. Kane, S. S. Yadav, J. Bitzegeio, S. B. Kutluay, T. Zang, S. J. Wilson, J. W. Schoggins, C. M. Rice, M. Yamashita, T. Hatziioannou, P. D. Bieniasz, MX2 is an interferon-induced inhibitor of HIV-1 infection. *Nature* **502**, 563–566 (2013).
14. S. J. D. Neil, T. Zang, P. D. Bieniasz, Tetherin inhibits retrovirus release and is antagonized by HIV-1 Vpu. *Nature* **451**, 425–430 (2008).
15. A. R. Sedaghat, J. German, T. M. Teslovich, J. Cofrancesco Jr., C. C. Jie, C. C. Talbot Jr., R. F. Siliciano, Chronic $CD4^+$ T-cell activation and depletion in human immunodeficiency virus type 1 infection: Type I interferon-mediated disruption of T-cell dynamics. *J. Virol.* **82**, 1870–1883 (2008).
16. G. Doitsh, N. L. K. Galloway, X. Geng, Z. Yang, K. M. Monroe, O. Zepeda, P. W. Hunt, H. Hatano, S. Sowinski, I. Muñoz-Arias, W. C. Greene, Cell death by pyroptosis drives CD4 T-cell depletion in HIV-1 infection. *Nature* **505**, 509–514 (2014).

17. S. Beq, S. Rozlan, S. Pelletier, B. Willems, J. Bruneau, J.-D. Lelievre, Y. Levy, N. H. Shoukry, R. Cheynier, Altered thymic function during interferon therapy in HCV-infected patients. *PLOS ONE* **7**, e34326 (2012).
18. F. J. Torriani, F. J. Torriani, M. Rodriguez-Torres, J. K. Rockstroh, E. Lissen, J. Gonzalez-García, A. Lazzarin, G. Carosi, J. Sasadeusz, C. Katlama, J. Montaner, H. Sette Jr., S. Passe, J. De Pamphilis, F. Duff, U. M. Schrenk, D. T. Dieterich, Peginterferon Alfa-2a plus ribavirin for chronic hepatitis C virus infection in HIV-infected patients. *N. Engl. J. Med.* **351**, 438–450 (2004).
19. A. S. Perelson, A. U. Neumann, M. Markowitz, J. M. Leonard, D. D. Ho, HIV-1 dynamics in vivo: Virion clearance rate, infected cell life-span, and viral generation time. *Science* **271**, 1582–1586 (1996).
20. J. M. Murray, A. D. Kelleher, D. A. Cooper, Timing of the components of the HIV life cycle in productively infected $CD4^+$ T cells in a population of HIV-infected individuals. *J. Virol.* **85**, 10798–10805 (2011).
21. S. G. Deeks, C. M. R. Kitchen, L. Liu, H. Guo, R. Gascon, A. B. Narváez, P. Hunt, J. N. Martin, J. O. Kahn, J. Levy, M. S. McGrath, F. M. Hecht, Immune activation set point during early HIV infection predicts subsequent $CD4^+$ T-cell changes independent of viral load. *Blood* **104**, 942–947 (2004).
22. A. L. Meditz, M. K. Haas, J. M. Folkvord, K. Melander, R. Young, M. McCarter, S. MaWhinney, T. B. Campbell, Y. Lie, E. Coakley, D. N. Levy, E. Connick, HLA-DR^+ $CD38^+$ $CD4^+$ T lymphocytes have elevated CCR5 expression and produce the majority of R5-tropic HIV-1 RNA in vivo. *J. Virol.* **85**, 10189–10200 (2011).
23. I. Rusinova, S. Forster, S. Yu, A. Kannan, M. Masse, H. Cumming, R. Chapman, P. J. Hertzog, INTERFEROME v2.0: An updated database of annotated interferon-regulated genes. *Nucleic Acids Res.* **41**, D1040–D1046 (2013).
24. X. Li, L. Xu, J. Li, B. Li, X. Bai, J. F. Strauss III, Z. Zhang, H. Wang, Otitis media in sperm-associated antigen 6 (*Spag6*)-deficient mice. *PLOS ONE* **9**, e112879 (2014).
25. J. Yu, M. Li, J. Wilkins, S. Ding, T. H. Swartz, A. M. Esposito, Y.-M. Zheng, E. O. Freed, C. Liang, B. K. Chen, S.-L. Liu, IFITM proteins restrict HIV-1 infection by antagonizing the envelope glycoprotein. *Cell Rep.* **13**, 145–156 (2015).
26. A. A. Compton, T. Bruel, F. Porrot, A. Mallet, M. Sachse, M. Euvrard, C. Liang, N. Casartelli, O. Schwartz, IFITM proteins incorporated into HIV-1 virions impair viral fusion and spread. *Cell Host Microbe* **16**, 736–747 (2014).
27. T. L. Foster, H. Wilson, S. S. Iyer, K. Coss, K. Doores, S. Smith, P. Kellam, A. Finzi, P. Borrow, B. H. Hahn, S. J. D. Neil, Resistance of transmitted founder HIV-1 to IFITM-mediated restriction. *Cell Host Microbe* **20**, 429–442 (2016).
28. X. Pan, H.-M. Baldauf, O. T. Keppler, O. T. Fackler, Restrictions to HIV-1 replication in resting $CD4^+$ T lymphocytes. *Cell Res.* **23**, 876–885 (2013).
29. Y. Zhou, H. Zhang, J. D. Siliciano, R. F. Siliciano, Kinetics of human immunodeficiency virus type 1 decay following entry into resting $CD4^+$ T cells. *J. Virol.* **79**, 2199–2210 (2005).
30. J. A. Zack, S. J. Arrigo, S. R. Weitsman, A. S. Go, A. Haislip, I. S. Y. Chen, HIV-1 entry into quiescent primary lymphocytes: Molecular analysis reveals a labile, latent viral structure. *Cell* **61**, 213–222 (1990).
31. K. Chen, J. Huang, C. Zhang, S. Huang, G. Nunnari, F.-x. Wang, X. Tong, L. Gao, K. Nikisher, H. Zhang, Alpha interferon potently enhances the anti-human immunodeficiency virus type 1 activity of APOBEC3G in resting primary CD4 T cells. *J. Virol.* **80**, 7645–7657 (2006).
32. H. Kambara, F. Niazi, L. Kostadinova, D. K. Moonka, C. T. Siegel, A. B. Post, E. Carnero, M. Barriocanal, P. Fortes, D. D. Anthony, S. Valadkhan, Negative regulation of the interferon response by an interferon-induced long non-coding RNA. *Nucleic Acids Res.* **42**, 10668–10680 (2014).
33. Y. Xu, M. Johansson, A. Karlsson, Human UMP-CMP kinase 2, a novel nucleoside monophosphate kinase localized in mitochondria. *J. Biol. Chem.* **283**, 1563–1571 (2008).
34. A. F. Weil, D. Ghosh, Y. Zhou, L. Seiple, M. A. McMahon, A. M. Spivak, R. F. Siliciano, J. T. Stivers, Uracil DNA glycosylase initiates degradation of HIV-1 cDNA containing misincorporated dUTP and prevents viral integration. *Proc. Natl. Acad. Sci. U.S.A.* **110**, E448–E457 (2013).
35. B. Guo, A. Godzik, J. C. Reed, Bcl-G, a novel pro-apoptotic member of the Bcl-2 family. *J. Biol. Chem.* **276**, 2780–2785 (2001).
36. M. Giam, T. Okamoto, J. D. Mintern, A. Strasser, P. Bouillet, Bcl-2 family member Bcl-G is not a proapoptotic protein. *Cell Death Dis.* **3**, e404 (2012).
37. M. S. Harper, K. Guo, K. Gibbert, E. J. Lee, S. M. Dillon, B. S. Barrett, M. D. McCarter, K. J. Hasenkrug, U. Dittmer, C. C. Wilson, M. L. Santiago, Interferon-α subtypes in an ex vivo model of acute HIV-1 Infection: Expression, potency and effector mechanisms. *PLOS Pathog.* **11**, e1005254 (2015).
38. A. Balagopal, A. J. Kandathil, Y. H. Higgins, J. Wood, J. Richer, J. Quinn, L. Eldred, Z. Li, S. C. Ray, M. S. Sulkowski, D. L. Thomas, Antiretroviral therapy, interferon sensitivity, and virologic setpoint in human immunodeficiency virus/hepatitis C virus coinfected patients. *Hepatology* **60**, 477–486 (2014).
39. D. Wodarz, M. A. Nowak, Mathematical models of HIV pathogenesis and treatment. *Bioessays* **24**, 1178–1187 (2002).
40. D. Finzi, R. F. Siliciano, Viral dynamics in HIV-1 Infection. *Cell* **93**, 665–671 (1998).
41. B. Li, C. N. Dewey, RSEM: Accurate transcript quantification from RNA-Seq data with or without a reference genome. *BMC Bioinformatics* **12**, 323 (2011).
42. N. Leng, J. A. Dawson, J. A. Thomson, V. Ruotti, A. I. Rissman, B. M. G. Smits, J. D. Haag, M. N. Gould, R. M. Stewart, C. Kendziorski, EBSeq: An empirical Bayes hierarchical model for inference in RNA-seq experiments. *Bioinformatics* **29**, 1035–1043 (2013).
43. Y. Hochberg, Y. Benjamini, More powerful procedures for multiple significance testing. *Stat. Med.* **9**, 811–818 (1990).

Acknowledgments: We would like to thank the participants of the study for contributing these invaluable samples; D. Mohr for expertise in library preparation and optimal sequencing; H. Zhang, Z. Freeman, and R. Veenhuis for helpful discussion and assistance with designing FACS protocols; and the organizers and instructors of the Quantitative Systems Immunology Summer School at Boston University and the Computational Immunology seminar series at Johns Hopkins University for introduction to the computational methods implemented in this investigation. **Funding:** This work was supported by the NIH (grant nos. R37 DA013806, R01 DA016078, K08 AI102696, and R01 HG006677), U.S. Army Research Office (grant no. W911NF-14-1-0490), and the Johns Hopkins University Center for AIDS Research (P30 AI094189). This publication was made possible by the Next Generation Sequencing Center at the Johns Hopkins Sidney Kimmel Comprehensive Cancer Center (P30 CA006973) and the Johns Hopkins Institute for Clinical and Translational Research (ICTR), which is funded, in part, by grant no. UL1 TR 000424-06 through a Clinical and Translational Science Award from the National Center for Advancing Translational Sciences (NCATS) (a component of the NIH), and NIH Roadmap for Medical Research. Its contents are solely the responsibility of the authors and do not necessarily represent the official view of the Johns Hopkins ICTR, NCATS, or NIH. **Author contributions:** R.E.-D. provided study concept and design, acquisition of data, analysis and interpretation of data, drafting of the manuscript, critical revision of the manuscript for important intellectual content, and statistical analysis. M.S., S.S., and N.S. performed acquisition of data and analysis and interpretation of data. M.C., J.R.B., R.F.S., J.N.B., and S.C.R. provided study concept and design, analysis and interpretation of data, and critical revision of the manuscript for important intellectual content. C.C. provided analysis and interpretation of data. F.B. provided analysis and interpretation of data. A.S. and S.J.W. provided analysis and interpretation of data and critical revision of the manuscript for important intellectual content. A.B. provided study concept and design, analysis and interpretation of data, critical revision of the manuscript for important intellectual content, and statistical analysis. D.L.T. obtained funding, provided study concept and design, analysis and interpretation of data, critical revision of the manuscript for important intellectual content, and statistical analysis. **Competing interests:** R.E.-D., D.L.T., and A.B. are inventors on a pending patent application (serial number PCT/US2017/019277, filed 24 February 2016) published as WO2017/147370, which claims priority to U.S. Provisional patent (application no. 62/299,086, filed 24 February 2015). The other authors declare that they have no competing interests. **Data and materials availability:** All data needed to evaluate the conclusions in the paper are present in the paper and/or the Supplementary Materials. All sequencing data are deposited in the NCBI sequence read archive (accession number SRP068424). Pegylated IFN-α2b was donated by Merck. Additional data and materials related to this paper may be requested from the authors and will be provided upon completion of a material transfer agreement.

Submitted 22 January 2018
Accepted 19 June 2018
Published 1 August 2018
10.1126/sciadv.aat0843

Citation: R. El-Diwany, M. Soliman, S. Sugawara, F. Breitwieser, A. Skaist, C. Coggiano, N. Sangal, M. Chattergoon, J. R. Bailey, R. F. Siliciano, J. N. Blankson, S. C. Ray, S. J. Wheelan, D. L. Thomas, A. Balagopal, CMPK2 and BCL-G are associated with type 1 interferon–induced HIV restriction in humans. *Sci. Adv.* **4**, eaat0843 (2018).

Science Advances

CMPK2 and BCL-G are associated with type 1 interferon–induced HIV restriction in humans

Ramy El-Diwany, Mary Soliman, Sho Sugawara, Florian Breitwieser, Alyza Skaist, Candelaria Coggiano, Neel Sangal, Michael Chattergoon, Justin R. Bailey, Robert F. Siliciano, Joel N. Blankson, Stuart C. Ray, Sarah J. Wheelan, David L. Thomas and Ashwin Balagopal

Sci Adv **4** (8), eaat0843.
DOI: 10.1126/sciadv.aat0843